Available online at www.sciencedirect.com
ScienceDirect
Journal of Magnetic Resonance 182 (2006) 221–228
JMR Journal of Magnetic Resonance
www.elsevier.com/locate/jmr

In vivo dynamic turnover of cerebral ^{13}C isotopomers from [U–^{13}C]glucose

Su Xu, Jun Shen *

Molecular Imaging Branch, National Institute of Mental Health, Bethesda, MD 20892, USA

Received 9 February 2006; revised 27 June 2006
Available online 21 July 2006

Abstract

An INEPT-based ^{13}C MRS method and a cost-effective and widely available 11.7 Tesla 89-mm bore vertical magnet were used to detect dynamic ^{13}C isotopomer turnover from intravenously infused [U–^{13}C]glucose in a 211 μL voxel located in the adult rat brain. The INEPT-based $^{1}H \rightarrow {}^{13}C$ polarization transfer method is mostly adiabatic and therefore minimizes signal loss due to B_1 inhomogeneity of the surface coils used. High quality and reproducible data were acquired as a result of combined use of outer volume suppression, ISIS, and the single-shot three-dimensional localization scheme built in the INEPT pulse sequence. Isotopomer patterns of both glutamate C4 at 34.00 ppm and glutamine C4 at 31.38 ppm are dominated first by a doublet originated from labeling at C4 and C5 but not at C3 (with $^{1}J_{C4C5} = 51$ Hz) and then by a quartet originated from labeling at C3, C4, and C5 (with $^{1}J_{C3C4} = 35$ Hz). A lag in the transition of glutamine C4 pattern from doublet-dominance to quartet dominance as compared to glutamate C4 was observed, which provides independent verification of the precursor–product relationship between neuronal glutamate and glial glutamine and a significant intercompartmental cerebral glutamate–glutamine cycle between neurons and glial cells.
Published by Elsevier Inc.

Keywords: Brain; ^{13}C MRS; Isotopomer; INEPT; Glutamate–glutamine cycle

1. Introduction

The ^{13}C labeling patterns of cerebral metabolites contain rich information of metabolic fluxes. For example, glutamate (and glutamine) with five carbon atoms has 2^5 or 32 possible labeling patterns, i.e., 32 possible ^{13}C isotopomers. Usually, groups of isotopomers are measured using high-resolution *in vitro* ^{13}C NMR spectroscopy [1–6] or proton-detected inverse NMR spectroscopy methods [7–9] or using mass spectrometry [10]. The additional information provided by isotopomers allows more sophisticated and realistic mathematical modeling of metabolic processes than the traditional methods based on radioactive tracers [11]. ^{13}C isotopomer measurement and analysis using *in vitro* NMR spectroscopy methods have made a significant impact to the studies of intermediary metabolism. For example, the selection of different exogenous substrates by heart [2], the contribution of different precursors to glucose and glycogen during hepatic gluconeogenesis [6], the relative activity of anaplerosis in perfused heart [1] and liver [12], as well as cerebral metabolic compartmentation [5,13,14] have been studied using *in vitro* ^{13}C isotopomer analysis of tissue extracts.

Parallel to the development of NMR-based *in vitro* ^{13}C isotopomer methods, significant progress has been made in advancing the *in vivo* ^{13}C MRS techniques [15–23]. With the current state-of-the-art of *in vivo* ^{13}C MRS techniques, modeling analysis of metabolism and intercompartmental glutamate–glutamine cycling has been limited to the use of the total signal intensity at each carbon position (e.g., the total ^{13}C signal intensities of glutamate C4 and glutamine C4) while the additional information contained in the ^{13}C isotopomers cannot be exploited due to the limited sensitivity and spectral resolution associated with many of the previous *in vivo* ^{13}C studies. Only limited attempts have

* Corresponding author. Fax: +1 301 480 2397.
E-mail address: shenj@intra.nimh.nih.gov (J. Shen).

1090-7807/$ - see front matter Published by Elsevier Inc.
doi:10.1016/j.jmr.2006.07.003

been made to utilize the *in vivo* isotopomer information [e.g., 24,25]. With the advent of high field magnets for animal studies, more sophisticated *in vivo* ^{13}C detection is increasingly feasible [25]. Here, we report an INEPT-based polarization transfer method [15,16,22,26] for *in vivo* detection of ^{13}C isotopomer turnover from intravenously infused [U-^{13}C]glucose at 11.7 Tesla. Significant improvement of the original INEPT method has been made in our laboratory by incorporating single-shot spatial localization of proton spins [15], outer volume suppression and adiabatic pulses for excitation, inversion and refocusing. The improved INEPT method was first implemented on a 4.7 Tesla scanner for studying monkey brain without using outer volume suppression or additional localization [22]. For the purpose of demonstrating the usefulness of cost-effective, widely available, 11.7 Tesla 89-mm bore vertical magnets, we used this INEPT method and uniformly [^{13}C]-labeled glucose ([U–^{13}C]glucose) as substrate in this study, which allows a straightforward demonstration of the product–precursor relationship between dynamic glutamate and glutamine isotopomer patterns. Our results provide independent verification of the concept that the intercompartmental glutamate-glutamine cycling process is a major metabolic flux. To the best of our knowledge, this is the first attempt to develop an *in vivo* $^{1}H \rightarrow {}^{13}C$ polarization transfer technique using the widely available, cost-effective 89-mm bore vertical magnets. As such, details of the technical aspect are given to facilitate implementation elsewhere. A preliminary account of this work has been presented at the fourteenth annual meeting of the International Society of Magnetic Resonance in Medicine (presentation 154).

2. Methods

2.1. MR hardware

All experiments were performed on a Bruker AVANCE spectrometer (Bruker Biospin, Billerica, MA) interfaced to an 11.7 Tesla 89-mm bore vertical magnet (Magnex Scientific, Abingdon, UK). The magnet is located in an unshielded room. It is equipped with a 57-mm i.d. gradient (Mini 0.5, Bruker Biospin, Billerica, MA, with a maximum gradient strength of 3.0 G/mm and a rise time of 100 μs) for *in vivo* studies of young adult rats. The Z_0 coil for the deuterium lock was used to compensate zero-order eddy current resulted from switching gradients. First order eddy current was compensated by preemphasis adjustments. No significant cross-preemphasis terms were found during a 1–1000 ms period after switching off a 50% 500 ms test gradient applied to each individual gradient axis. An integrated RF coils/head holder system was constructed and mounted on a half-cylindrical plastic cradle. The ^{1}H and ^{13}C RF coils were coplanar and made of single-sided printed circuit board. The inner loop is the ^{13}C coil with an inner diameter and conductor width of 10.8 and 4.3 mm, respectively. The outer loop is the ^{1}H coil with an inner diameter and conductor width of 23.6 and 5.4 mm, respectively. To provide the necessary RF shielding, the main body of the RF probe/animal handling system was built using an aluminum tube with an outer diameter of 56.6 mm. The lower end of the system was an aluminum interface box through which RF cables, ventilation tubes, rectal thermal probe, and catheters were connected. A similar design of the RF probe/animal handling system for proton and Proton-Observed, Carbon-13-Edited spectroscopy experiments of rat brain using the vertical 89-mm bore magnet was descried previously [27]. The RF probe/animal handling system is suitable for rat head fixation, body support, physiology maintenance, coil tuning and RF shielding. It allows maintenance of normal physiology over prolonged period despite of increased cardiac load and blood draining associated with vertically positioned rats [27]. It is mechanically interfaced to the magnet using an adaptor ring which allows vertical and angular position adjustments. The loaded isolation between ^{1}H and ^{13}C coils (S21), which have a large frequency separation of 375 MHz, is −30.6 dB at 125 MHz and −31.2 dB at 500 MHz, respectively. Standard Bruker filters were used. A broadband low-pass filter was used in ^{13}C channel whose insertion loss at 125 MHz was less than 0.5 dB. Its rejection at 500 MHz was greater than 80 dB. In the proton channel, a broad-band high-pass filter was used with an insertion loss at 500 MHz less than 0.5 dB and rejection at 125 MHz greater than 60 dB. No noise injection was found in the ^{13}C channel due to proton decoupling.

2.2. Pulse sequence design

The main portion of the pulse sequence was constructed based on INEPT. The RF pulses for polarization transfer were also used for three-dimensional spatial localization of the thermal equilibrium proton signals. As depicted in Fig. 1, the proton magnetization was first excited using a

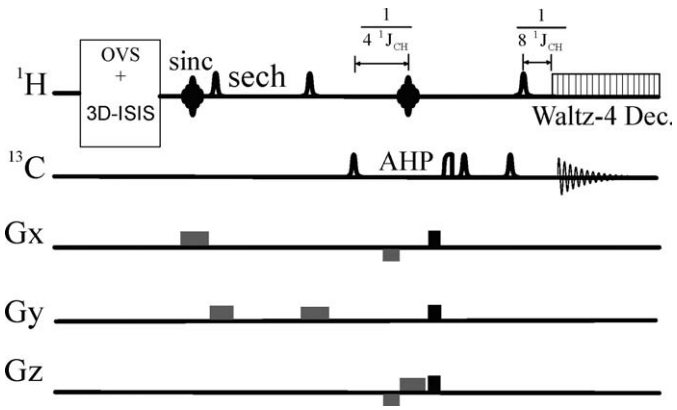

Fig. 1. The pulse sequence for proton localized, INEPT-based $^{1}H \rightarrow {}^{13}C$ polarization transfer. RF pulses in polarization transfer were used for three-dimensional spatial localization through proton. OVS, outer volume suppression; ISIS, image-selected *in vivo* spectroscopy; sinc, five-lobe sinc pulse; sech, hyperbolic secant pulse; AHP, adiabatic half-passage pulse. Black rectangles, crusher gradients and gray rectangles, slice selection gradients. The nominal $1/4^{1}J_{CH}$ and $1/8^{1}J_{CH}$ delays were also indicated.

90° 520 μs, five-lobe sinc pulse applied along x axis of the RF rotating frame with simultaneous slice selection along the x dimension. Immediately after the sinc pulse, an adiabatic hyperbolic secant pulse (2-ms, phase factor = 3, 1% truncation) was executed. The slice selection direction of the sech pulse was along the y axis. An adiabatic pure phase spin echo of the selected y slice was formed by the use of a second, identical slice-selective sech pulse [28]. Proton echo-time was set to 9.2 ms. The evolution of ^{1}H-^{13}C J couplings was reintroduced by applying a third sech pulse (1-ms, phase factor = 5, 1% truncation) to the ^{13}C channel which allows the formation of the antiphase 2^1H_x–$^{13}C_z$ term inside the column at the interception of the x and y slices after a nominal delay of $0.25/^1J_{HC}$ [22]. Then a second 90° sinc pulse (520 μs, five-lobe) was applied along y axis of the RF rotating frame to the proton channel to generate the desired ^{1}H–^{13}C longitudinal two-spin order. The nominal $0.25/^1J_{HC}$ was empirically optimized to be 1953 μs from the midpoint of the ^{13}C sech pulse to the midpoint of the second sinc pulse by maximizing the polarization transferred signal from a phantom sample containing ^{13}C-enriched [4-^{13}C]glutamate. The second sinc pulse also acts as a slice-selective universal rotator pulse for the spatial z dimension [29]. As a result, the ^{1}H–^{13}C longitudinal two-spin order was formed only in the voxel defined by two sinc pulses for x and z slices and the pair of sech pulses for the y slice. All transverse magnetization was suppressed by crusher gradients placed after the second 90° sinc pulse. The rewinding gradient of the second sinc pulse for the 2^1H_x–$^{13}C_z \rightarrow 2^1H_z$–$^{13}C_z$ transformation was not needed. The $^1H \rightarrow {}^{13}C$ polarization transfer was realized by the use of a spectrally and spatially nonselective adiabatic half-passage pulse (500 μs, [30]) to convert the ^{1}H–^{13}C longitudinal two-spin order into antiphase ^{1}H-^{13}C magnetization (2^1H_z–$^{13}C_y$). The antiphase ^{1}H–^{13}C magnetization was then rephased. During the rephasing period, the chemical shift evolution and B_0 inhomogeneity were refocused using a similar adiabatic double spin echo scheme with a pair of identical sech pulses but without slice-selection gradients (1-ms, phase factor = 5, 1% truncation). The evolution of the ^{1}H–^{13}C J couplings was reintroduced by applying one more sech pulse (2-ms, phase factor = 3, 1% truncation) to the ^{1}H channel before data recording. The nominal delay between the ^{1}H sech pulse and the start of data acquisition should be $0.125/^1J_{HC}$ for optimal detection of methylene carbons. The nominal $0.125/^1J_{HC}$ delay was empirically optimized to be 1140 μs from the midpoint of the proton sech pulse to the start of the data acquisition by maximizing the polarization transferred signal from the phantom sample containing ^{13}C-enriched [4-^{13}C]glutamate. WALTZ-4 ^{1}H decoupling pulse (9.6 ms) was applied during data acquisition with the ^{1}H carrier frequency for decoupling centered at ~2.35 ppm. Prior to the start of the polarization transfer sequence, an outer volume suppression scheme and three-dimensional ISIS localization were employed to ensure a clean baseline free of contamination from subcutaneous lipid signals. The proton outer volume suppression scheme also used sech pulses (90° nominal flip angle, 2 ms, phase factor = 5, 1% truncation) along the x (10 mm slab), $-x$ (10 mm slab), y (3 mm slab), $-y$ (5 mm slab), z (10 mm slab), $-z$ (10 mm slab) directions, and crusher gradients. In-between the outer volume suppression scheme and polarization transfer, the sech-based three-dimensional ISIS localization of protons (2 ms, phase factor = 3, 1% truncation) was used to further suppress contamination from subcutaneous lipid signals.

2.3. Animal preparation

Male Sprague–Dawley rats (180–200 g, $n = 6$) fasted overnight with free access to drinking water were studied as approved by the National Institute of Mental Health Animal Care and Use Committee. The rats were orally intubated and ventilated with a mixture of 70% N_2O/30% O_2 and 1.5% isoflurane. The left femoral artery was cannulated where plasma samples were withdrawn every 30 min for monitoring arterial blood gases, pH, plasma glucose concentration using a blood analyzer (Bayer Rapidlab 860, East Walpole, MA), and for monitoring arterial blood pressure. Two femoral veins were also cannulated, one for continuous infusion of α-chloralose (initial dose: 80 mg/kg supplemented with a constant rate infusion at 25.4 mg/kg/h throughout the experiment), the other for infusion of [U–^{13}C]glucose (99% enrichment, Cambridge Isotope Laboratories, Andover, MA, 20% wt/vol) first at 8 ml/h over 5 min followed by infusion at a lower rate which was adjusted over a small range to maintain plasma glucose concentration at 17.15 ± 0.75 mM and a fractional enrichment of ~96%. The ^{13}C fractional enrichment of plasma glucose was determined using a broadband inverse gradient probe (BBI, 50 G/mm on the z-axis) and high-resolution NMR spectroscopy of plasma PCA extracts as described previously [31]. After surgery, isoflurane was discontinued. Rectal temperature was maintained at ~37.5 °C using an external pump for water circulation (BayVoltex, Modesto, CA). Normal arterial blood physiological parameters were maintained by small adjustments of respiration rate and volume ($pH = 7.39 \pm 0.02$, $pCO_2 = 40 \pm 3$ mmHg, $pO_2 > 100$ mmHg, mean arterial blood pressure = 140–172 mmHg). End-tidal CO_2, tidal pressure of ventilation, and heart rate were also monitored.

2.4. In vivo MR procedures

Three-slice (coronal, horizontal, and sagittal) scout RARE images (FOV = 2.5 cm, slice thickness = 1 mm, TR/TE = 200/15 ms, rare factor = 8, 128 × 128 data matrix) were acquired for positioning the RF probe/animal handling system inside the Mini 0.5 gradient insert such that the gradient isocenter was about 0–1 mm posterior to bregma for selection of a $7.5 \times 3.75 \times 7.5$ mm^3 (211 μL) spectroscopy voxel. The rat brain was shimmed as described previously using the FASTMAP/FLATNESS methods [32, and references therein]. *In vivo* ^{13}C NMR

spectra were acquired with the proton-localized, INEPT-based polarization transfer method described above. The pulse sequence was embedded in a Bruker AU program. The AU program allows on-the-flight adjustment of RF power to optimize suppression of outer volume signals using one dimensional profile of tissue water from the proton channel along x, y, and z dimensions, respectively. For the $^{1}H \rightarrow {}^{13}C$ polarization transfer experiment, recycle delay was set to 2.5 s. For each data block of ^{13}C data, 720 scans were accumulated over 30 min. After acquisition of each data block, a fixed 5 min interval was allocated for re-shimming to maintain optimal B_0 homogeneity over a total experimental duration of 5 h and 10 min.

3. Results

A typical time course spectra of dynamic isotopomer turnover from the 211 μL voxel of a rat was shown in Fig. 2. The accumulated FID of each data block was zero-filled to 16 K. Ten Hz exponential line-broadening was applied prior to Fourier transform. Zero-order and minor first order phase corrections were made. No baseline correction was found necessary. To demonstrate the high consistency of the data across different animals, the data blocks for each 30-min time interval from the six rats were summed. The results were displayed in Fig. 3. As shown in Figs. 2 and 3, the time courses of ^{13}C label incorporation into C2, C3, and C4 of glutamate; C2, C3 and C4 of glutamine; C2 and C3 of aspartate; and C6 of *N*-acetyl-aspartate as well as the fine isotopomer structures arising from homonuclear ^{13}C–^{13}C *J*-couplings could be clearly detected over the 20–60 ppm range. Isotopomer patterns of aspartate C3 at 37.08 ppm, glutamate C4 at 34.00 ppm, glutamine C4 at 31.38 ppm, glutamate C3 at 27.45 ppm + glutamine C3 at 26.78 ppm, glutamate C2 at 55.33 ppm + glutamine C2 at 54.87 ppm, and NAA C6 at 22.52 ppm selected from spectra of individual rats were expanded and shown in Fig. 4a–f. The isotopomer patterns observed *in vivo* are consistent with the known ^{13}C–^{13}C homonuclear *J* couplings previously detected *in vitro* [5]. At early time points, the predominant isotopomer at glutamate C4 at 34.00 ppm is Glu4D45 contributed by [4,5-^{13}C]glutamate which is formed by the condensation of [1, 2-^{13}C]acetyl-CoA with unlabeled oxaloacetate during the first turn of the TCA cycle. Then Glu4Q gradually dominates the isotopomer pattern of glutamate C4 as the labeling of the carbonyl carbon of oxaloacetate increases over time. Mostly due to the relatively small difference between $^{1}J_{C4C5}$ (51 Hz) and $^{1}J_{C3C4}$ (35 Hz) of glutamate, the two central lines of Glu4Q coalesced after application of the 10 Hz exponential line-broadening. As shown in Figs. 2 and 3, the temporal dynamics of the isotopomer patterns of glutamine C4 is similar to glutamate C4. However, a noticeable lag in the turnover of glutamine C4 isotopomer from the doublet-dominated pattern to the quartet dominated pattern can be appreciated visually in Figs. 2 and 3. For example, in Fig. 3 during the 175–205 min interval with both glutamate C4 and glutamine C4 isotopomers at high

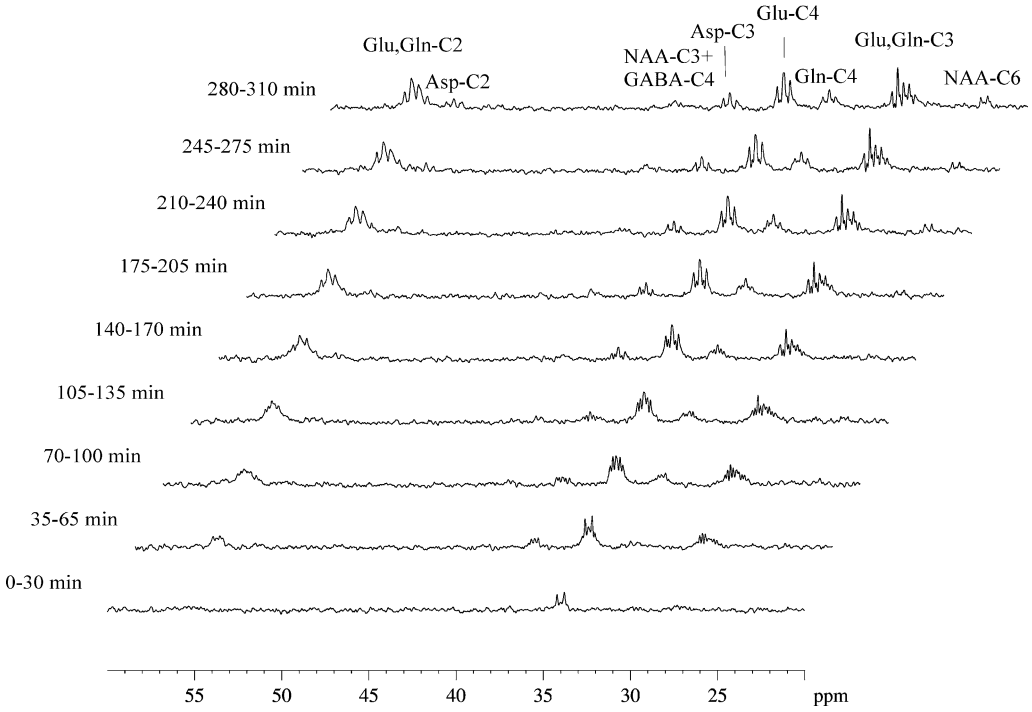

Fig. 2. Typical time course spectra of dynamic isotopomer turnover from the $7.5 \times 3.75 \times 7.5$ mm^3 voxel in a single rat detected *in vivo* using the 89-mm bore 11.7 Tesla vertical magnet. The accumulated FID of each data block was zero-filled to 16 K. Ten Hz exponential line-broadening was applied prior to Fourier transform. There was a 5-min gap between two adjacent acquisitions which was used for re-shimming when necessary. Glu, glutamate; Gln, glutamine; GABA, γ-aminobutyric acid; Asp, aspartate; NAA, *N*-acetylaspartate.

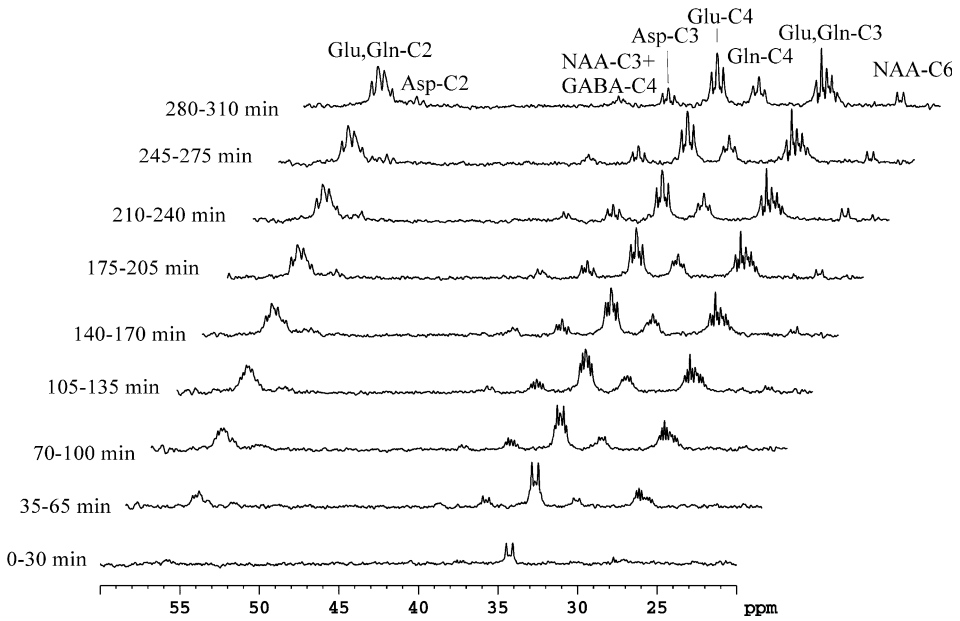

Fig. 3. For demonstration of high reproducibility, the summed time course spectra in the 20–60 ppm range were shown for comparison with Fig. 2. Each individual spectrum was the addition of data blocks from the six rats and the same 30-min time interval. Identical data acquisition and processing parameters were used for all animals. Glu, glutamate; Gln, glutamine; GABA, γ-aminobutyric acid; Asp, aspartate; NAA, *N*-acetylaspartate.

sensitivity, the two Gln4D45 resonance lines are approximately at the same height as that of the two outer resonance lines of Gln4Q. In comparison, during the same time interval, the relative contribution of Glu4D45 to the glutamate C4 isotopomer is much less with the height of the two outer resonance lines of Glu4Q reaching that of Glu4D45 during the earlier 140–170 min time interval.

Despite the use of 11.7 Tesla, the upfield resonance line of Glu3T still overlaps with the downfield resonance line of Gln3T (see Fig. 4d). At early time points, there is a large contribution from Glu3D and Gln3D to the isotopomers of glutamate C3 at 27.45 ppm and glutamine C3 at 26.78 ppm. At later time points, the contribution from Glu3T to glutamate C3 and that from Gln3T become dominant over that from Glu3D and Gln3D. A similar lag in the domination of Gln3T in the isotopomer pattern of glutamine C3 when compared to that of Glu3T in the isotopomer pattern of glutamate C3 can be seen in Figs. 2 and 3. Similar to the cases of glutamate C4 and glutamine C4, the isotopomer patterns of glutamate C2 at 55.33 ppm and glutamine C2 at 54.87 ppm are dominated by Glu2D12 + Glu2D23 + Glu2Q and Gln2D12 + Gln2D23 + Gln2Q, respectively. At later time points, Glu2Q and Gln2Q become the dominant forms of glutamate C2 and glutamine C2, respectively. Because the chemical shift difference between glutamate C2 at 55.33 ppm and glutamine C2 at 54.87 ppm at 11.7 Tesla is very similar to $^{1}J_{C1C2}$ of glutamate and glutamine, a pseudo quartet was detected at 55.09 ppm during the 280–310 min interval with the central two resonance lines from Glu2Q overlapping the downfield resonance line of Gln2Q and the central two resonance lines from Gln2Q overlapping the upfield resonance line of Glu2Q (Fig. 4e). Significant *in vivo* turnover of *N*-acetylaspartate (NAA) C6, manifested by the conspicuous signal of NAA6D at 22.52 ppm, was also detected in Figs. 2, 3, 4f, consistent with previous in vivo observations of NAA synthesis [33].

4. Discussion

Vertical, 89-mm bore magnets were manufactured initially for magic angle spinning solid state NMR spectroscopy applications. Recently, this type of magnets, which are widely available and relatively cost-effective compared to the wider and horizontal bore magnets, have been increasingly used to image mice and small rats. Recently, we have demonstrated *in vivo* proton and POCE MRS data of excellent quality using a vertical, 89-mm bore magnet at 11.7 Tesla, the highest field strength at which in vivo spectroscopy of rodent brain has ever been attempted [27,31,32]. The results of current report extend the usefulness of vertical, 89-mm bore magnets to include *in vivo* localized ^{13}C MRS.

This investigation also suggests that numerous isotopomers metabolized from intravenously infused [U–^{13}C]glucose could be locally measured in the rat brain *in vivo* with a temporal resolution suitable for dynamic isotopomer analysis, which could provide additional constraints for extraction of metabolic fluxes using metabolic modeling. Metabolic modeling can also take into account of variations in arterial input function. For example, the Glu4D/Glu4Q ratio was determined to be 1.09 ± 0.13 (mean ± SEM, $n = 6$) at the 70–100 min period. The variations in isotopomer pattern across different animals include contributions from spectral noise, inter-animal variability, as well as variations in arterial input function. Quantitative mod-

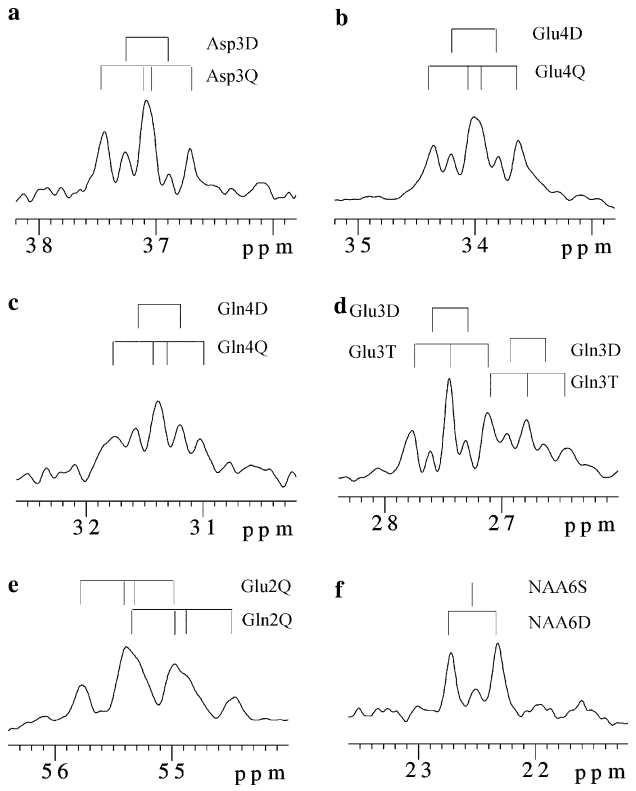

Fig. 4. Isotopomer patterns selected from spectra of individual rats. (a) Aspartate C3 at 37.08 ppm. $^{1}J_{C3C4} = 51$ Hz, $^{1}J_{C2C3} = 36$ Hz. Time period: 175–205 min. (b) Glutamate C4 at 34.00 ppm. $^{1}J_{C4C5} = 51$ Hz, $^{1}J_{C3C4} = 35$ Hz. Time period: 140–170 min. (c) Glutamine C4 at 31.38 ppm. $^{1}J_{C4C5} = 48$ Hz, $^{1}J_{C3C4} = 35$ Hz. Time period: 140–170 min. (d) Glutamate C3 at 27.45 ppm. $^{1}J_{C3C4} = 35$ Hz, $^{1}J_{C2C3} = 35$ Hz. Glutamine C3 at 26.78 ppm. $^{1}J_{C3C4} = 35$ Hz, $^{1}J_{C2C3} = 35$ Hz. Time periods: 175–205 min. (e) Glutamate C2 at 55.33 ppm. $^{1}J_{C1C2} = 53$ Hz, $^{1}J_{C2C3} = 35$ Hz. Glutamine C2 at 54.87 ppm. $^{1}J_{C1C2} = 53$ Hz, $^{1}J_{C2C3} = 35$ Hz. Time period: 280–310 min. (f) *N*-acetylaspartate C6 at 22.52 ppm. $^{1}J_{C5C6} = 50$ Hz. Time period: 280–310 min. Q, quartet; T, triplet; D, doublet. The chemical shift assignments were obtained from ref. [43].

eling of the turnover time course of individual isotopomers using metabolic compartments comprised of glutamatergic neurons and glia is out of the scope of this technical report due to the complexity of the issues and will be pursued in the future. Instead, only a qualitative discussion of some salient features of the isotopomer patterns and turnover processes detected *in vivo* will be conducted here. To simplify isotopomer patterns high plasma fractional enrichment of [U–^{13}C]glucose (~96%) was used in this study. As a result, the fraction of unlabeled acetyl-CoA should be very low [24]. At later time points the unlabeled carbons in glutamate, glutamine and aspartate are largely replaced by ^{13}C labels. Consequently, Glu4Q, Gln4Q, Glu3T, Gln3T, Glu2Q, Gln2Q and Asp3Q became the dominant isotopomers at the end of the [U–^{13}C]glucose infusion experiment. This is in contrast to early *in vitro* experiments which used very low ^{13}C fractional enrichments [14,40]. For example, with the plasma [U–^{13}C]glucose fractional enrichment at <~7%, glutamate C3 is overwhelmingly dominated by Glu3S while Glu3T was not observed at all [40].

According to the recently revitalized concept of glutamate-glutamine cycling between neurons and glia [17,23,31,34–37], the turnover dynamics of glutamine ^{13}C isotopomer patterns is expected to be similar to that of glutamate except with a lag. This lag was indeed observed in Figs. 2 and 3 with a delayed domination by the Gln4Q quartet in glutamine C4 and a similarly delayed domination by the Gln3T triplet in glutamine C3. Therefore, the observed dynamic turnover kinetics of glutamate and glutamine isotopomers confirms the concepts of the precursor-product relationship between glutamate and glutamine and a significant cerebral glutamate–glutamine cycle, which were established previously based on the total signal intensities of [^{13}C]-labeled glutamate and glutamine.

Using a 9.4 Tesla 310-mm bore horizontal magnet, *in vivo* isotopomer patterns of glutamate C4, glutamine C4 and glutamate + glutamine C3 acquired after infusing 70% [U–^{13}C]glucose have also been reported recently [25], which are similar to those shown in Fig. 4. A slightly better chemical shift separation of glutamate C3 from the overlapping glutamine C3 was achieved at 11.7 Tesla as expected. In contrast to previous *in vitro* studies using [U–^{13}C]glucose with low fractional enrichment [14,38–40], no significant singlets (e.g., Glu3S, Glu2S, Gln3S, Gln2S) were observed in the current study due to the use of close to 100% fractional enrichment of plasma [U–^{13}C]glucose. Due to large susceptibility effect in vivo, the spectral resolution achieved in this study is poorer than that obtainable in vitro. For example, the $^{1}J_{C3C4}$ coupling constant of glutamate has been reported to be 34.5 Hz. The relatively broad in vivo linewidth does not allow meaningful detection of a 0.5 Hz frequency difference. The broad in vivo linewidth is also expected to obscure very small singlets. Note that the INEPT method per se, which can be used to differentiate methine, methylene and methyl carbons, does not suppress ^{13}C singlets.

Due to the spatial constraint imposed by the 57-mm i.d. gradient insert, only the co-planar ^{13}C {^{1}H} surface coil system was found to be viable. The large frequency separation between ^{1}H and ^{13}C resonance frequencies reduces the mutual coupling between the two surface coils. Careful electromagnetic-geometrical design led to minimized coupling via the tune/match circuitries and between RF cables. As a result, excellent overall performance of the INEPT-based polarization transfer technique was achieved (see Figs. 2 and 3). The INEPT-based pulse sequence depicted in Fig. 1 is inherently single-shot since the two five-lobe sinc pulses with slice selection along x and z and the double adiabatic spin echo sech pulses with slice selection along y provide single-shot spatial localization of proton spins. To compensate the degradation of the excitation profile of the five-lobe sinc pulses caused by the B_1 inhomogeneity of the single-loop proton surface coil, two additional localization schemes (outer volume suppression and three-dimensional ISIS) were added. This was found necessary to acquire high-quality and reproducible data using the current hardware by completely eliminating contamination from

subcutaneous lipid signals. Due to the wide dispersion of ^{13}C chemical shifts, the chemical shift error associated with direct ^{13}C localization would be intolerably large. Because of the use of proton localization, even using the 11.7 Tesla 89-mm bore vertical magnet, the largest localization error in the pulse sequence described in Fig. 1 is only ±0.6 mm along the x and z dimensions over the 22.52 (*N*-acetylaspartate C6)–55.33 (glutamate C2) ppm range of interest. The ±0.6 mm localization error along the x and z dimensions was caused by the relatively long sech pulses used in additional localization by ISIS. The corresponding localization error in the y dimension is ±0.3 mm. Based on considerations of equal signal intensity of ^{13}C in CH and that of ^{13}C in CH_2 as well as less transverse relaxation loss, INEPT is more suitable for *in vivo* ^{13}C MRS studies of glucose metabolism than DEPT [15]. With nonadiabatic pulses and surface or half-volume coils, DEPT has the advantages of using less RF pulses, therefore, smaller susceptibility to signal loss caused by B_1 inhomogeneity. The only nonadiabatic pulses in the INEPT sequence shown in Fig. 1 are the two nominal 90° sinc pulses. Since the effect of B_1 inhomogeneity is proportional to flip angles, the two nominal 90° sinc pulses generated by the larger proton surface coil are least susceptible to the effect of B_1 inhomogeneity among all pulses used in the INEPT sequence per se. They were made nonadiabatic to make the built-in spatial localization single-shot so as to minimize any subtraction errors [22].

To achieve high sensitivity and low spatial localization error *in vivo*, the use of $^1H \rightarrow {}^{13}C$ heteronuclear polarization transfer or Hartmann–Hahn transfer (a.k.a. *J* cross-polarization) techniques is advantageous although they make it practically impossible to directly observe isotopomers of carboxylic carbons (e.g., C1 and C5 of glutamate and glutamine; C1 and C4 of aspartate; C5 of N-acetylaspartate). Carboxylic carbons and HCO_3^- have been previously detected *in vivo* using direct ^{13}C MRS [19,20,22]. The use of long-range ^1H–^{13}C *J* coupling for polarization transfer or heteronuclear Hartmann–Hahn transfer is not feasible because of the relatively short *in vivo* T_2 or $T_{1\rho}$. The time period used in polarization transfer to refocus the antiphase 2^1H_z–$^{13}C_y$ coherence is also detrimental to the detection of ^{13}C isotopomers because of the concomitant ^{13}C–^{13}C homonuclear *J* evolution. The ^{13}C double adiabatic spin echo sech pulses used in Fig. 1 have a bandwidth of 10 kHz or 79.5 ppm. Therefore, the carboxylic carbons of glutamate, glutamine, aspartate, and *N*-acetylaspartate resonating in the 174.27–181.8 ppm range are not affected by the 180° ^{13}C pulses. Consequently, homonuclear ^{13}C–^{13}C *J* evolution between carboxylic carbon and the neighboring methylene and methine carbons is refocused; while the homonuclear ^{13}C–^{13}C *J* evolution among the methylene and methine carbons is not refocused, the latter causes significant distortions in isotopomer patterns. The characteristics of such distortions are mainly dependent on pulse sequence and timing parameters and, to a much lesser degree, on field strength. Comparing to the isotopomer patterns of glutamate C4 in Fig. 4b, the corresponding isotopomer acquired using DEPT [25] has a smaller separation between Glu4Q and Glu4D45 resonance lines, and the two inner resonance lines of its Glu4Q are more apart. The relative positions of the resonance lines in Fig. 4b appear to be closer to those detected from brain extracts *in vitro* using direct ^{13}C MRS [41]. Isotopomer distortions associated with INEPT and DEPT pulse sequences can be taken into account during quantification using deconvolution algorithms such as LCModel [40]. Alternative to the polarization transfer techniques which require ^{13}C detection, many ingenious methods developed by the high-resolution NMR community can be adapted for *in vivo* proton detection of ^{13}C isotopomers. Of them, HMQC-TOCSY and HSQC [7–9] methods have already been used for proton detection of ^{13}C isotopomers *in vitro*. Since one of the major issues for proton detection of complex ^{13}C isotopomers is the separation of contributions from different ^{13}C isotopomers, combining proton-detection with ^{13}C–^{13}C homonuclear multiple quantum filtering of isotopomers [42] could provide an attractive option.

Acknowledgments

The authors thank Dr. Steve Li for constructing and evaluating the $^{13}C\{^1H\}$ RF probe/animal handling system, Mr. Wenjun Zhu for performing animal surgery, Dr. Jehoon Yang for assistance in analyzing the plasma samples, and the anonymous reviewers for helpful comments. This research was supported by the Intramural Research Program of the NIH, NIMH.

References

[1] C.R. Malloy, A.D. Sherry, F.M. Jeffrey, Carbon flux through citric acid cycle pathways in perfused heart by ^{13}C NMR spectroscopy, FEBS Lett. 212 (1987) 58–62.

[2] C.R. Malloy, A.D. Sherry, F.M. Jeffrey, Evaluation of carbon flux and substrate selection through alternate pathways involving the citric acid cycle of the heart by ^{13}C NMR spectroscopy, J. Biol. Chem. 263 (1988) 6964–6971.

[3] C.R. Malloy, J.R. Thompson, F.M. Jeffrey, A.D. Sherry, Contribution of exogenous substrates to acetyl coenzyme A: measurement by ^{13}C NMR under non-steady-state conditions, Biochemistry 29 (1990) 6756–6761.

[4] C.R. Malloy, A.D. Sherry, F.M. Jeffrey, Analysis of tricarboxylic acid cycle of the heart using ^{13}C isotope isomers, Am. J. Physiol. 259 (1990) H987–H995.

[5] S. Cerdan, B. Kunnecke, J. Seelig, Cerebral metabolism of [1,2-$^{13}C_2$]acetate as detected by *in vivo* and *in vitro* ^{13}C NMR, J. Biol. Chem. 265 (1990) 12916–12926.

[6] F.M. Jeffrey, A. Rajagopal, C.R. Malloy, A.D. Sherry, ^{13}C -NMR: a simple yet comprehensive method for analysis of intermediary metabolism, Trends Biochem. Sci. 16 (1991) 5–10.

[7] W. Willker, U. Flogel, D. Leibfritz, A $^1H/^{13}C$ inverse 2D method for the analysis of the polyamines putrescine, spermidine and spermine in cell extracts and biofluids, NMR Biomed. 11 (1998) 47–54.

[8] R.A. Carvalho, F.M. Jeffrey, A.D. Sherry, C.R. Malloy, C isotopomer analysis of glutamate by heteronuclear multiple quantum coherence-total correlation spectroscopy (HMQC-TOCSY), FEBS Lett. 440 (3) (1998) 382–386.

[9] R.A. Carvalho, P. Zhao, C.B. Wiegers, F.M. Jeffrey, C.R. Malloy, A.D. Sherry, TCA cycle kinetics in the rat heart by analysis of ^{13}C isotopomers using indirect ^{1}H, Am. J. Physiol. Heart Circ. Physiol. 281 (2001) H1413–H1421.

[10] M.E. Jennings 2nd, D.E. Matthews, Determination of complex isotopomer patterns in isotopically labeled compounds by mass spectrometry, Anal. Chem. 77 (2005) 6435–6444.

[11] A.D. Sherry, F.M. Jeffrey, C.R. Malloy, Analytical solutions for ^{13}C isotopomer analysis of complex metabolic conditions: substrate oxidation, multiple pyruvate cycles, and gluconeogenesis, Metab. Eng. 6 (2004) 12–24.

[12] B.M. Jucker, J.Y. Lee, R.G. Shulman, *In vivo* ^{13}C NMR measurements of hepatocellular tricarboxylic acid cycle flux, J. Biol. Chem. 273 (1998) 2187–12194.

[13] B. Kunnecke, S. Cerdan, J. Seelig, Cerebral metabolism of [1,2-^{13}C2]glucose and [U–^{13}C 4]3-hydroxybutyrate in rat brain as detected by ^{13}C NMR spectroscopy, NMR Biomed. 6 (1993) 264–277.

[14] A. Lapidot, A. Gopher, Cerebral metabolic compartmentation. Estimation of glucose flux via pyruvate carboxylase/pyruvate dehydrogenase by ^{13}C NMR isotopomer analysis of D-[U–^{13}C]glucose metabolites, J. Biol. Chem. 269 (1994) 27198–271208.

[15] H. Watanabe, Y. Ishihara, K. Okamoto, K. Oshio, T. Kanamatsu, Y. Tsukada, *In vivo* 3D localized ^{13}C spectroscopy using modified INEPT and DEPT, J. Magn. Reson. 134 (1998) 214–222.

[16] H. Watanabe, Y. Ishihara, K. Okamoto, K. Oshio, T. Kanamatsu, Y. Tsukada, 3D localized ^{1}H–^{13}C heteronuclear single-quantum coherence correlation spectroscopy *in vivo*, Magn. Reson. Med. 43 (2000) 200–210.

[17] J. Shen, D.L. Rothman, Magnetic resonance spectroscopic approaches to studying neuronal: glial interactions, Biol. Psychiatry. 52 (2002) 694–700.

[18] J. Shen, K.F. Petersen, K.L. Behar, P. Brown, T.W. Nixon, G.F. Mason, O.A.C. Petroff, G.I. Shulman, R.G. Shulman, D.L. Rothman, Determination of the rate of the glutamate/glutamine cycle in the human brain by *in vivo* ^{13}C NMR, Proc. Natl. Acad. Sci. USA 96 (1999) 8235–8240.

[19] S. Bluml, A. Moreno, J.H. Hwang, B.D. Ross, 1-^{13}C glucose magnetic resonance spectroscopy of pediatric and adult brain disorders, NMR Biomed. 14 (2001) 19–32.

[20] S. Bluml, A. Moreno-Torres, B.D. Ross, [1-^{13}C]glucose MRS in chronic hepatic encephalopathy in man, Magn. Reson. Med. 45 (2001) 981–993.

[21] V. Lebon, K.F. Petersen, G.W. Cline, J. Shen, G.F. Mason, S. Dufour, K.L. Behar, G.I. Shulman, D.L. Rothman, Astroglial contribution to brain energy metabolism in humans revealed by ^{13}C nuclear magnetic resonance spectroscopy: elucidation of the dominant pathway for neurotransmitter glutamate repletion and measurement of astrocytic oxidative metabolism, J. Neurosci. 22 (2002) 1523–1531.

[22] S. Li, Z. Chen, Y. Zhang, M. Lizak, J. Bacher, R.B. Innis, J. Shen, *In vivo* single-shot, proton-localized ^{13}C MRS of rhesus monkey brain, NMR Biomed. 18 (2005) 560–569.

[23] N. Chhina, E. Kuestermann, J. Halliday, L.J. Simpson, I.A. Macdonald, H.S. Bachelard, P.G. Morris, Measurement of human tricarboxylic acid cycle rates during visual activation by ^{13}C magnetic resonance spectroscopy, J. Neurosci. Res. 66 (2001) 737–746.

[24] J. Shen, R.A. de Graaf, V. Lebon, D.L. Rothman, Determination of the isotopic composition of acetyl CoA in the human brain using ^{13}C isotopomers, in: Proceedings of the ISMRM, 10th Scientific Meeting, Honolulu, 2002, p. 963.

[25] P.G. Henry, I. Tkac, R. Gruetter, ^{1}H-localized broadband ^{13}C NMR spectroscopy of the rat brain *in vivo* at 9.4 T, Magn. Reson. Med. 50 (2003) 684–692.

[26] G.A. Morris, R. Freeman, Enhancement of nuclear magnetic resonance signals by polarization transfer, J. Am. Chem. Soc. 101 (1979) 760–762.

[27] S. Li, J. Shen, Integrated RF probe for *in vivo* multinuclear spectroscopy and functional imaging of rat brain using an 11.7 Tesla 89-mm bore vertical microimager, MAGMA 18 (2005) 119–127.

[28] S. Conolly, G. Glover, D. Nishimura, A. Macovski, A reduced power selective adiabatic spin-echo pulse sequence, Magn. Reson. Med. 18 (1991) 28–38.

[29] J. Shen, Slice-selective J-coupled coherence transfer using symmetric linear phase pulses: applications to localized GABA spectroscopy, J. Magn. Reson. 163 (2003) 73–80.

[30] J. Shen, Use of amplitude and frequency transformations to generate adiabatic pulses of wide bandwidth and low RF power deposition, J. Magn. Reson. Ser. B 112 (1996) 131–140.

[31] J. Yang, J. Shen, *In vivo* evidence for reduced cortical glutamate–glutamine cycling in rats treated with the antidepressant/antipanic drug phenelzine, Neuroscience 135 (2005) 927–937.

[32] Z. Chen, S.S. Li, J. Yang, D. Letizia, J. Shen, Measurement and automatic correction of high order B_0 inhomogeneity in the rat brain at 11.7 Tesla, Magn. Reson. Imag. 22 (2004) 835–842.

[33] A. Moreno, B.D. Ross, S. Bluml, Direct determination of the *N*-acetyl-L-aspartate synthesis rate in the human brain by ^{13}C MRS and [1-^{13}C]glucose infusion, J. Neurochem. (2001) 347–350.

[34] N.R. Sibson, J. Shen, G.F. Mason, D.L. Rothman, K.L. Behar, R.G. Shulman, Functional energy metabolism: *in vivo* ^{13}C-NMR spectroscopy evidence for coupling of cerebral glucose consumption and glutamatergic neuronal activity, Dev. Neurosci. 20 (1998) 321–330.

[35] D.L. Rothman, N.R. Sibson, F. Hyder, J. Shen, K.L. Behar, R.G. Shulman, *In vivo* nuclear magnetic resonance spectroscopy studies of the relationship between the glutamate-glutamine neurotransmitter cycle and functional neuroenergetics, Philos. Trans. R Soc. Lond. B Biol. Sci. 354 (1999) 1165–1177.

[36] J. Shen, ^{13}C MRS studies of alterations in glutamate neurotransmission, Biol. Psychiatry. 59 (2006) 883–887.

[37] K. Kanamori, B.D. Ross, R.W. Kondrat, Glial uptake of neurotransmitter glutamate from the extracellular fluid studied in vivo by microdialysis and ^{13}C NMR, J. Neurochem. 83 (2002) 682–695.

[38] B. Kalderon, S.H. Korman, A. Gutman, A. Lapidot, Estimation of glucose carbon recycling in children with glycogen storage disease: a ^{13}C NMR study using [U–^{13}C]glucose, Proc. Natl. Acad. Sci. USA 86 (1989) 4690–4694.

[39] A. Lapidot, S. Haber, Effect of acute insulin-induced hypoglycemia on fetal versus adult brain fuel utilization, assessed by ^{13}C MRS isotopomer analysis of [U–^{13}C]glucose metabolites, Dev. Neurosci. 22 (2000) 444–455.

[40] S. Haber, A. Lapidot, Energy fuel utilization by fetal versus young rabbit brain: a ^{13}C MRS isotopomer analysis of [U–^{13}C]glucose metabolites, Brain Res. 896 (2001) 102–117.

[41] P.G. Henry, G. Oz, S. Provencher, R. Gruetter, Toward dynamic isotopomer analysis in the rat brain *in vivo*: automatic quantitation of ^{13}C NMR spectra using LCModel, NMR Biomed. 16 (2003) 400–412.

[42] J. Weigelt, G. Otting, ^{1}H-detected INEPT-INADEQUATE at natural ^{13}C abundance, J. Magn. Reson. Ser. A 113 (1995) 28–130.

[43] W.M.T. Fan, Metabolite profiling by one- and two-dimensional NMR analysis of complex mixtures, Prog. NMR Spectrosc. 28 (1996) 161–219.